Inorganic Chemistry

Facile Fabrication of CeO_2-Al_2O_3 Hollow Sphere with Atomically Dispersed Fe via Spray Pyrolysis

Xin-Pu Fu, Wen-Zhu Yu, Meng-Yuan Li, Rui Si,* Chao Ma,* and Chun-Jiang Jia*

Read Online

ACCESS | Metrics & More | Article Recommendations | Supporting Information

ABSTRACT: A facile spray pyrolysis method is introduced to construct the hollow CeO_2-Al_2O_3 spheres with atomically dispersed Fe. Only nitrates and ethanol were involved during the one-step preparation process using the ultrasound spray pyrolysis approach. Detailed explorations demonstrated that differences in the pyrolysis temperature of the precursors and heat transfer are crucial to the formation of the hollow nanostructure. In addition, iron species were in situ atomically dispersed on the as-formed CeO_2-Al_2O_3 hollow spheres via this strategy, which demonstrated promising potential in transferring syn-gas to valuable gasoline products.
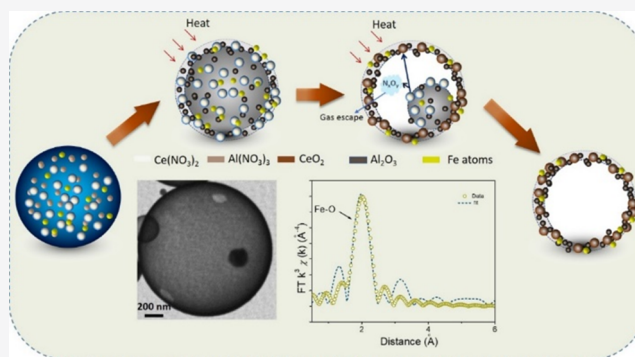
INTRODUCTION

Metal oxides with hollow nanostructure have received increasing attention due to their promising potential in various fields, including catalysis, energy storage, drug delivery, and sensor.[1−6] The traditional approaches to fabricate hollow structures usually comprise hard template way or soft template.[3,7,8] However, the derived pollution and complexity during preparation procedures strongly inhibit the wider application of template routes. Other assembly strategies, including Kirkendall process,[9] Oswald ripening process,[10] decomposition of metal−organic frameworks,[11] and coordination polymers,[12] have been successfully applied in producing hollow nanostructure. Nevertheless, most of them are still obstructed by their sophisticated synthetic procedure. Therefore, the formation of a hollow structure via a facile strategy is desirable.

Among various oxides, cerium dioxide (CeO_2) has long been significantly attractive in catalytic application[13−20] because of its environmental friendliness, spontaneous Ce^{3+}/Ce^{4+}, and superior surface property.[13,21,22] A fine synergistic effect can be potentially identified during the catalysis process in the form of ceria-based composites when ceria is combined with metals or metal oxides.[23] Therefore, M/CeO_2 were widely used as catalysts for numerous catalytic reactions, including reforming,[24] oxidation of volatile organic compounds (VOC),[25] water−gas shift (WGS) reaction,[23] CO (preferential) oxidation,[26] oxidative dehydrogenation,[27] and so on. Nano-sized CeO_2 was frequently utilized in the catalysis process owing to its abundant exposure to the surface, while the easy aggregation severely hindered its efficiency. Thus, the construction of a stable hollow structure with CeO_2 nanoparticles would be greatly beneficial to optimize its capacity in the catalytic application.[24,28−31] However, the facile route for the construction of the CeO_2 hollow structure via template-free method has been rarely developed so far.[32]

Herein, we reported a facile strategy to fabricate hollow nanospheres comprising dominant CeO_2 and minor Al_2O_3 phases with the aid of the spray pyrolysis technique.[33−43] The differentiated decomposition temperatures for cerium nitrate and auxiliary precursor (aluminum nitrate) are vital in the formation of hollow morphology. Through this approach, atomically dispersed Fe atoms are in situ anchored in the CeO_2-Al_2O_3 hollow spheres in one step, which the atomic dispersion metal sites have demonstrated widely potential in catalytic applications.[44−46] The as-prepared Fe single atoms in the CeO_2-Al_2O_3 hollow spheres (Fe-SA/CeO_2-Al_2O_3) demonstrated promising catalytic performance in the Fischer−Tropsch reaction, which is the key technology to generate fuels from syngas. The CO conversion at 330 °C is ∼50% coupling with good stability during a long-term test. In addition, the selectivity of 66% for the desired light olefins and C_{5+}. This work provided a general approach for synthesizing CeO_2-based hollow structures with highly dispersed metal sites.
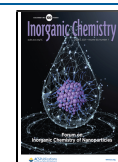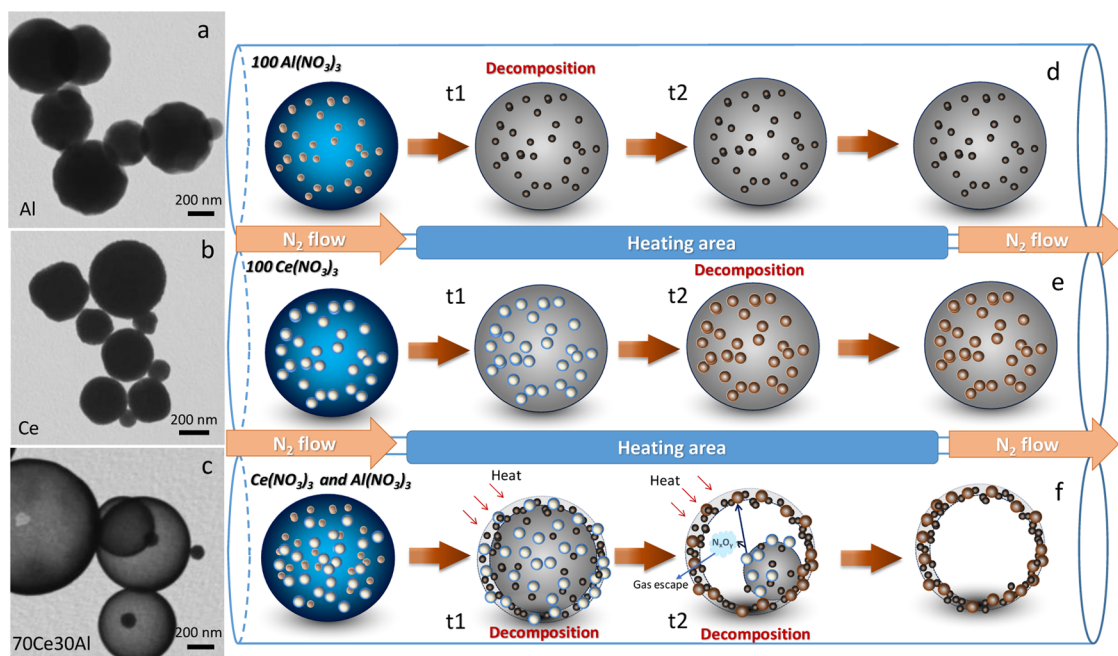
Figure 1. TEM images of the CeO_2-Al_2O_3 spheres with various Ce/Al ratios, (a) 100%Al, (b) 100%Ce, and (c) 70%Ce/30%Al. Scale bar: 200 nm. Plausible schematic illustration of the formation process for (d) 100%Al, (e) 100%Ce, and (f) 70%Ce/30%Al.

■ EXPERIMENTAL SECTION

Catalyst Preparation. *Materials.* All chemicals were directly used without further modifications. Cerium nitrate hexahydrate (Ce-$(NO_3)_3$·$6H_2O$), aluminum nitrate nonahydrate (Al$(NO_3)_3$·$9H_2O$), and sodium hydroxide (NaOH) were provided by Tianjin Kermal Chemical Reagent Factory.

Preparation of CeO_2-Al_2O_3 Hollow Spheres. The ultrasound spray pyrolysis technique is used to synthesize the CeO_2 dominant hollow spheres. First, mixed Ce$(NO_3)_3$·$6H_2O$ and Al$(NO_3)_3$·$9H_2O$ (total amount is 8 mmol and molar ratios of Ce/Al were changed with 100/0, 50/50, 70/30, and 0/100) were added into 80 mL ethanol. After stirring for 10 min, the transparent solution was subsequently transferred to the ultrasonic humidifier, which would generate microspheres via the aerosol-spraying progress. After that, the atomized spray flowed inside a 90 cm long glass tube by pure N_2 flow (150 mL·min^{-1}), which was preheated by a tube furnace at 450 °C. Finally, the as-prepared powder samples were further dried in an oven at 80 °C overnight.

Preparation of Fe-SA/CeO_2-Al_2O_3 Hollow Spheres. Similarly, Fe-SA/CeO_2-Al_2O_3 was prepared with the same method mentioned above, where the ratio of Fe/Ce/Al was changed to 10/70/30. Additional alkali etching (1 M NaOH solution) treatment was taken on the collected sample for 24 h.

Characterizations. Ex situ X-ray diffraction (XRD) test was conducted on a powder diffractometer (PANalytical B.V. X′pert3, 40 kV, 40 mA), coupled with Cu Kα1 radiation (α = 0.15406 nm).

The transmission electron microscopy (TEM) test was conducted on an FEI Tecnai F20 instrument (200 kV). A JEOL ARM200F microscope, coupled with a probe-forming spherical-aberration corrector and Gatan image filter (Quantum 965), was used to record the aberration-corrected high-angle annular dark-field scanning transmission electron microscopy (HAADF-STEM) images. The electron energy-loss spectroscopy (EELS) was also recorded on the same equipment, which provided the elemental mapping results from the Fe-$L_{2,3}$, Ce-$M_{4,5}$, and O-K edges.

X-ray photoelectron spectroscopy (XPS) analysis was conducted on an Axis Ultra XPS spectrometer (Kratos, U.K.) using 225 W Al Kα radiation. The binding energies were corrected via calibrating the C 1s peak at 284.8 eV.

The ex situ X-ray absorption fine structure (XAFS) spectra of Fe K-edge (E_0 = 7112 eV) for both fresh and spent iron−ceria catalysts were recorded at BL14W1 beamline of Shanghai Synchrotron Radiation Facility. Two operation modes were used, with one under the "top-up" mode at 3.5 GeV coupled with a 220 mA constant current and the other one operated at 20-ID-B beamline of Advanced Photon Source (APS) of Argonne National Laboratory (ANL), which was operated under a top-up mode at 7.0 GeV (constant current: 100 mA). A Lytle ion chamber or a four-channel Vortex silicon drift detector recorded the XAFS data under fluorescence mode. The pure Fe foil was used to calibrate the data. Also, the as-collected data was extracted and fitted by Athena and Artemis codes. For the X-ray absorption near-edge structure (XANES) profile, to normalize the absorption energy, the coefficients of experimental absorption as a function for energies $\mu(E)$ were processed by background subtraction and normalization steps. For the extended X-ray absorption fine structure (EXAFS) profile, the Fourier transform (FT) data in R space proceeded with the use of the first-shell approximation or metallic Fe model for the Fe−O/Fe−O−Fe/Fe−O−Ce or Fe−Fe coordination. The passive electron factors (S_0^2) were determined by fitting the experimental Fe foil data and fixing the Fe−Fe coordination number (CN) to 8 + 6 and subsequently fixing for the following analysis of the measured samples. The other parameters that allowed us to change during the fit process comprise the parameters related to the electronic properties (E_0) and the values of the local structure environment including CN, bond distance (R), and Debye−Waller (D.W.) factor around the absorbing atoms.

Catalytic Measurements. The Fischer−Tropsch synthesis (FTS) reaction was conducted on a fixed-bed flow reactor with a gas mixture of 47% CO, 47% H_2, and 6%N_2. Catalyst powders (0.08 g) were diluted with 0.5 g of SiO_2 particles (20−40 mesh) before the test. The FTS measurements at 330 °C were carried out under high pressure of 2 MPa with a pretreatment at 380 °C for 3 h in 10%H_2/Ar. The gas hourly space velocity (GHSV) of the reaction was set at 13 500 cm^3·h^{-1}·g$_{cat}^{-1}$. The product and reactant in the gas phase were detected online using a gas chromatograph (GC-9160, Shanghai, China). The C_1−C_4 ranged hydrocarbons were analyzed using a Plot Al_2O_3 capillary column with a flame ionization detector (FID); however, CO, CO_2, CH_4, and N_2 were analyzed using a Porapak Q and 5A molecular sieve-packed column with a thermal conductivity detector (TCD). All hydrocarbons were analyzed using GC-9160 with a PONA capillary column and a flame ionization detector (FID). To calculate the CO conversion, 6%N_2 in syngas was used as an internal

standard. The selectivity of the products was all based on carbon. The selectivity of CO_2, CH_4, C_2-C_4, and C_{5+} is calculated on the basis of all used CO molecules. The catalytic activity (Fe time yield, FTY) is defined as the amount of converted CO moles per gram of Fe per second.

■ RESULTS AND DISCUSSION

The oxides powders were continuously produced using the spray pyrolysis equipment. The morphology of the as-prepared nanospheres is strongly affected by the ratio of precursors. When only independent $Ce(NO_3)_3$ or $Al(NO_3)_3$ was used as a feedstock, solid nanospheres with a diameter of 100−500 nm could be observed in the TEM images (Figure 1a,b). In contrast, the hollow inner was clearly identified as the Ce/Al ratio changed to 50:50 (Figure S1), whereas the spherical shape was irregular. After optimizing the ratio as 70:30, which is the ratio of the spheres with a hollow structure was above 90%, a smooth and integrated outline was fabricated as shown in Figure 1c (Figure S2). Considering that the co-presence of both $Ce(NO_3)_3$ and $Al(NO_3)_3$ was indispensable for constructing a hollow inner, the difference in the decomposition temperature (T_d) of the two precursors is envisioned as a plausible induction for the hollow structure. In detail, ΔT_d of $Ce(NO_3)_3$ and $Al(NO_3)_3$ is as high as ∼130 K with the separated T_d values of 570 and 440 K, respectively.[47] The correlation between ΔT_d and the formation of hollow inner was further evidenced by the solid feature for the combinations of $Ce(NO_3)_3$ and $Co(NO_3)_2$ or $Cu(NO_3)_2$ (Figure S3), whose ΔT_d values were only ∼17 and ∼7 K, respectively (Table S1). A similar phenomenon was also got in the formation of the Co_3O_4-Al_2O_3 hollow nanostructure over the combination of $Co(NO_3)_2$ and $Al(NO_3)_3$, coupling with a ΔT_d value of ∼100 K.

During the ultrasound atomization process, the mixture in ethanol solution was atomized to a lot of small droplets, where drastic gas−liquid reaction is conducting. Therefore, considering the strong correlation between heating transfer, ΔT_d, and the formation of a hollow structure, we proposed a plausible formation mechanism of the CeO_2-Al_2O_3 spheres as follows. As shown in Figure 1d,e, the independent $Ce(NO_3)_3$ or $Al(NO_3)_3$ precursor decomposed at different stages after atomizing into the tube with the aid of N_2 flow, the $Al(NO_3)_3$ pyrolyzed at an earlier time of t_1, and $Ce(NO_3)_3$ decomposed at a subsequent time of t_2. The interval between t_1 and t_2 provided the condition for the formation of an outer surface layer of Al_2O_3 with the rapid evaporation of ethanol at first. Then, the decomposed N_xO_y from $Ce(NO_3)_3$ created a relatively high inner gas pressure, which promoted the substance inside to spread to the outer layer (Figure 1f). In addition, the working temperatures demonstrated a considerable effect on the formation of a hollow structure, where the relatively higher temperature (450 °C) was favorable for the fabrication of smaller sizes (Figure S4). In addition, a gradual evolution from hollow to yolk-shell structure was found to increase the amount of surfactant incorporated in the solvent (Figure 2). Considering the change in the thermal conductivity for the precursor solvent, the evolution of the inner structure implied the possible role of heating transfer in constructing a hollow structure. Furthermore, it provides a facile strategy to modulate the morphology of nanospheres.

The powder X-ray diffraction (XRD) demonstrated only the face-centered cubic (fcc) structure of CeO_2 without any phase of Al_2O_3 for the as-prepared CeO_2-Al_2O_3 spheres (Figure S5a).
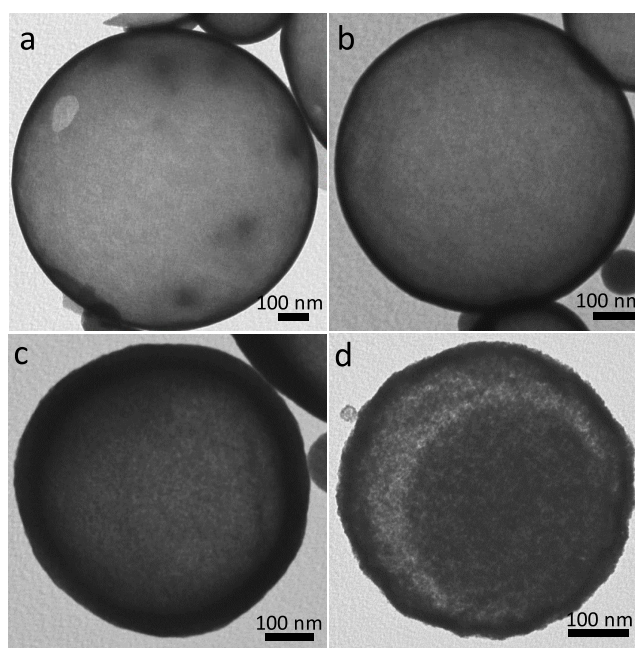

Figure 2. TEM images of CeO_2-Al_2O_3 (Ce/Al = 70:30) hollow spheres with different contents of F127 during the synthesis process: (a) 0 F127, (b) 0.05 F127, (c) 0.4 F127, and (d) 0.8 F127.

Compared with pure CeO_2, no detectable shift could be observed for diffraction peak, indicating the absence of lattice contraction induced by the doping of Al atoms (Figure S5b). As shown in the scanning electron microscopy (SEM) images (Figure S6), the hollow morphology of the CeO_2-Al_2O_3 spheres was also identified through the broken holes on the surface. In addition, the porous property of the hollow spheres was confirmed by the Brunauer−Emmett−Teller (BET) measurement (Figure S7). Therefore, the hollow sphere comprising abundant small CeO_2 nanoparticles and amorphous Al_2O_3 was fabricated via a template-free approach. Furthermore, through in situ mixings, various kinds of metals, such as Fe, Co, Ni, Ru, Pd, etc., can be well dispersed over this CeO_2 dominant hollow sphere, which would be beneficial for wide catalytic applications.

In this work, Fe was in situ fixed on the CeO_2-Al_2O_3 hollow spheres with the same approach. X-ray photoelectron spectroscopy (XPS) was used to measure the elemental composition of the CeO_2-Al_2O_3 composites. The Fe/Ce/Al ratio of the surface layer (∼5 nm) for the composites without any treatment determined by XPS is 10/58/32 (Figure S8). Additional etching treatment by NaOH solution was conducted over Fe-SA/CeO_2-Al_2O_3 for better exposure of metal sites, in which the estimated atomic ratio of Fe/Ce/Al is changed from 10/58/32 to 15/70/15 based on XPS results (Figure S9). Correspondingly, the mass ratio (wt %) of the components (Fe_2O_3/CeO_2/Al_2O_3) was changed from 5.9/80.5/13.6% to 6.4/87.4/6.2%, confirming the dramatic decrease in the Al content. Compared with CeO_2-Al_2O_3 hollow spheres, the morphology remained nearly unchanged after introducing Fe atoms as revealed in the TEM images (Figure 3a,b). The atomic-resolution HAADF-STEM image shown in Figure 3c exhibited that the ceria was highly crystallized with clear lattice fringes. With the aid of STEM-EELS, the presence of Fe, Ce, and O elements was observed with a uniform dispersion over the field of view (Figure 3d).
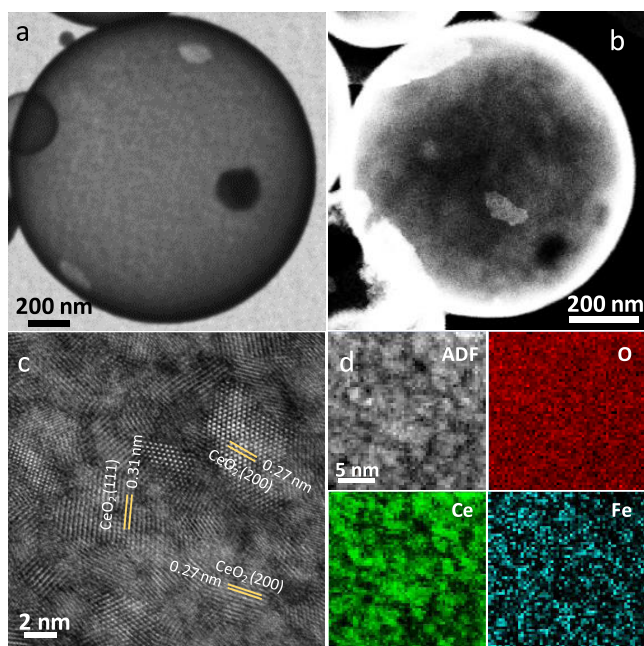
Figure 3. (a) Overview TEM image, (b) HAADF-STEM image, (c) atomic-resolution HAADF image, and (d) STEM-EELS mapping results of the as-prepared Fe-SA/CeO$_2$-Al$_2$O$_3$ hollow sphere.

To further identify the specific structure around the measured Fe atoms, the XAFS technique was used to investigate the iron–ceria samples, which were elementally sensitive to determine both electronic and local structures.[48] As shown in XANES results (Figure 4a), the Fe K-edge
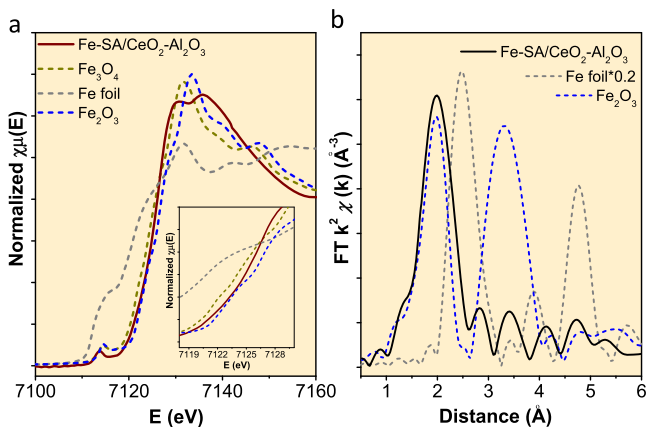
Figure 4. (a) XANES spectra, where the insert is the magnified spectra and (b) Fourier transform (FT) of the Fe K-edge EXAFS spectra of Fe-SA/CeO$_2$-Al$_2$O$_3$ hollow sphere.

spectrum for fresh Fe-SA/CeO$_2$-Al$_2$O$_3$ is between Fe$_2$O$_3$ and Fe$_3$O$_4$, indicating that the oxidation state of Fe atoms is between Fe$_2$O$_3$ and Fe$_3$O$_4$. The accurate coordination information of the Fe atom was analyzed by EXAFS (Figure 4b). Only primary Fe–O contribution in R space at 1.96 Å was clearly identified, without the observation of Fe–Fe shell (R = 2.46 Å) in the first shell or the Fe–O–Fe shell in the second shell (R = 3.32 Å), proving the atomic dispersion with only Fe–O coordination for the Fe atoms on the CeO$_2$-Al$_2$O$_3$ hollow spheres. Based on the fitting result (Figure S10), the

coordination number (CN) of Fe–O in the first shell was 4.3 ± 0.9.

To preliminarily value the potential of the as-prepared hollow composites in catalytic applications, we evaluated it as a catalyst for the Fischer–Tropsch synthesis (FTS) reaction, which is one of the key technologies to convert syn-gas to environmental fuel and the conventional reaction condition is tough.[37,49] Figure 5a illustrates the catalytic steady test over the as-prepared Fe-SA/CeO$_2$-Al$_2$O$_3$ at 330 °C for 40 h, as well as the reference catalysts Fe/Al$_2$O$_3$ and Fe/CeO$_2$ with solid feature. A gradual increase in CO conversion was observed in the initial 15 h for the Fe-SA/CeO$_2$-Al$_2$O$_3$ catalyst, indicative of a potential activation process induced in the initial stage, which might be ascribed to the phase transformation from oxides to carbides.[49,50] Subsequently, the CO conversion reached a plateau with a constant conversion of ca. 50%, implying relatively good stability under tough reaction conditions. The CO conversion of Fe-SA/CeO$_2$-Al$_2$O$_3$ catalyst obviously surpassed that of Fe/CeO$_2$ and Fe/Al$_2$O$_3$ (53 vs 5% or 10%), where the mass loading of Fe is comparable for these catalysts (4.5 wt % vs 4.6 or 5.1%). The superior catalytic performance of Fe-SA/CeO$_2$-Al$_2$O$_3$ spheres might indicate the strength of its hollow structure. The CO conversation rate normalized by Fe mass (Fe-time yield, FTY) is 827 μmol·g^{-1}· s^{-1} at 330 °C, which is a moderately good catalytic performance (Table S3).[51−53] The selectivity for the desired light olefins (C$_{2=}$–C$_{4=}$) and C$_{5+}$ hydrocarbons were 27.0 and 38.7%, respectively (Figure 5b; 65.7% in total, selectivity calculated basing on all hydrocarbons).

In addition, the chain-growth probability (α) obtained from the Anderson–Schulz–Flory (ASF) model for Fe-SA/CeO$_2$-Al$_2$O$_3$ was 0.51 (Figure S11). As shown in Figure S12a, a small number of spheres were broken after the FTS reaction and the predominant spheres are integrate. The only detectable crystalline phase after the reaction is CeO$_2$ (Figure S12b), which is the same as that of the fresh one. To further confirm the potential correlation between the catalytic performance and structural features, the spent Fe-SA/CeO$_2$-Al$_2$O$_3$ catalyst after the reaction at 330 °C was analyzed by XAFS. As shown in Figure 6a, the oxidation state of Fe atoms was close to Fe$_3$O$_4$ based on the XANES results, which became slightly reduced as compared with the samples before reaction. Considering the gradual activation process during the FTS reaction, these reduced Fe atoms might be the active sites. The presence of atomically dispersed Fe sites was confirmed by the isolated presence of Fe–O coordination in the first shell as shown in EXAFS results (R = 1.95 ± 0.02 Å, CN = 4.0 ± 0.8; Figure 6b), demonstrating their good stability on the surface of hollow CeO$_2$ sphere, which should be the origin of the satisfactory catalytic stability under FTS reaction condition.

CONCLUSIONS

In summary, we have developed a facile strategy for the fabrication of a CeO$_2$-Al$_2$O$_3$ hollow sphere by the spray pyrolysis technique. Comprehensive characterizations showed that the difference in the decomposition temperatures of two precursors and the heating transfer played crucial roles in the formation of hollow morphology. With the aid of this method, the Fe element could be simply and atomically dispersed over the CeO$_2$ hollow spheres synchronously during the synthesis process. The as-prepared Fe-SA/CeO$_2$-Al$_2$O$_3$ hollow sphere revealed the CO conversion rate of 827 μmol·g^{-1}·s^{-1} at 330 °C couplings with a selectivity of 67% for the desired light olefins
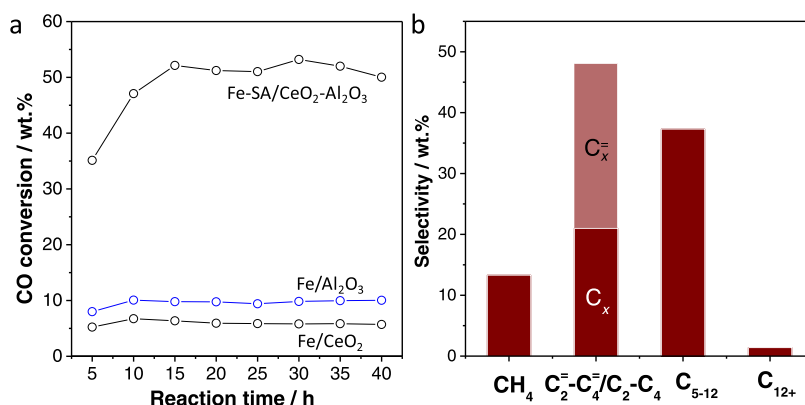
Figure 5. (a) Catalytic CO conversion of the Fe-SA/CeO$_2$-Al$_2$O$_3$ hollow sphere, Fe/Al$_2$O$_3$ and Fe/CeO$_2$ nanospheres. (b) Product selectivity of Fe-SA/CeO$_2$-Al$_2$O$_3$ hollow sphere. The CH$_4$, C$_2$−C$_4$, and C$_{5+}$ selectivity was calculated based on all hydrocarbons excluding CO$_2$. Reaction condition: T = 330 °C, H$_2$/CO = 1:1, P = 20 bar, F = 18 mL·min^{-1}, and W_{catal} = 0.08 g.
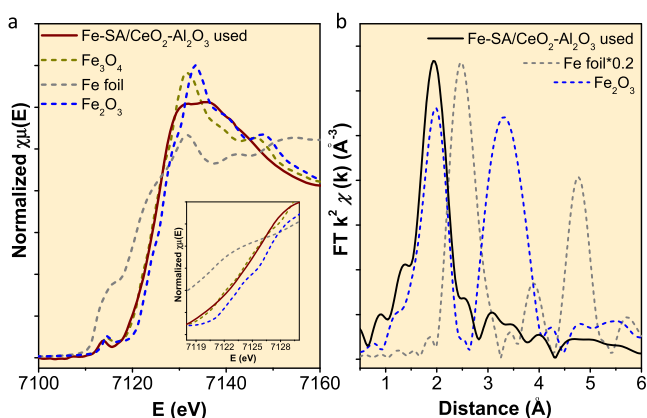
Figure 6. (a) XANES spectra, which in the inset is magnified spectra, and (b) Fourier transform (FT) of the Fe K-edge EXAFS of Fe-SA/CeO$_2$-Al$_2$O$_3$ hollow sphere after FTS reaction at 330 °C.

and C$_{5+}$. This work provided a facile and general route for synthesizing hollow CeO$_2$ structures with highly dispersed metal sites.

■ ASSOCIATED CONTENT

Ⓢ Supporting Information

The Supporting Information is available free of charge at https://pubs.acs.org/doi/10.1021/acs.inorgchem.1c00194.

Experimental details, additional TEM images, and XRD and XPS results (PDF)

■ AUTHOR INFORMATION

Corresponding Authors

Rui Si − *Shanghai Synchrotron Radiation Facility, Shanghai Institute of Applied Physics, Chinese Academy of Sciences, Shanghai 201204, China;* ⓘ orcid.org/0000-0003-0732-9688; Email: sirui@mail.sysu.edu.cn

Chao Ma − *College of Materials Science and Engineering, Hunan University, Changsha 410082, China;* ⓘ orcid.org/0000-0001-8599-9340; Email: cma@hnu.edu.cn

Chun-Jiang Jia − *Key Laboratory for Colloid and Interface Chemistry, Key Laboratory of Special Aggregated Materials, School of Chemistry and Chemical Engineering, Shandong University, Jinan 250100, China;* ⓘ orcid.org/0000-0002-4254-5100; Email: jiacj@sdu.edu.cn

Authors

Xin-Pu Fu − *Key Laboratory for Colloid and Interface Chemistry, Key Laboratory of Special Aggregated Materials, School of Chemistry and Chemical Engineering, Shandong University, Jinan 250100, China;* ⓘ orcid.org/0000-0001-8379-0789

Wen-Zhu Yu − *Key Laboratory for Colloid and Interface Chemistry, Key Laboratory of Special Aggregated Materials, School of Chemistry and Chemical Engineering, Shandong University, Jinan 250100, China*

Meng-Yuan Li − *Key Laboratory for Colloid and Interface Chemistry, Key Laboratory of Special Aggregated Materials, School of Chemistry and Chemical Engineering, Shandong University, Jinan 250100, China*

Complete contact information is available at:
https://pubs.acs.org/10.1021/acs.inorgchem.1c00194

■ REFERENCES

(1) Huo, L.; Liu, B.; Li, H.; Cao, B.; Hu, X.-c.; Fu, X.-p.; Jia, C.; Zhang, J. Component Synergy and Armor Protection Induced Superior Catalytic Activity And Stability of Ultrathin Co-Fe Spinel Nanosheets Confined in Mesoporous Silica Shells for Ammonia Decomposition Reaction. *Appl. Catal., B* **2019**, *253*, 121−130.

(2) Song, G.; Chao, Y.; Chen, Y.; Liang, C.; Yi, X.; Yang, G.; Yang, K.; Cheng, L.; Zhang, Q.; Liu, Z. All-in-One Theranostic Nanoplatform Based on Hollow TaO$_x$ for Chelator-Free Labeling Imaging, Drug Delivery, and Synergistically Enhanced Radiotherapy. *Adv. Funct. Mater.* **2016**, *26*, 8243−8254.

(3) Sun, Q.; Wang, N.; Yu, J.; Yu, J. C. A Hollow Porous CdS Photocatalyst. *Adv. Mater.* **2018**, *30*, No. e1804368.

(4) Wang, J.; Cui, Y.; Wang, D. Design of Hollow Nanostructures for Energy Storage, Conversion and Production. *Adv. Mater.* **2019**, *31*, No. e1801993.

(5) Zou, Y.; Chen, S.; Sun, J.; Liu, J.; Che, Y.; Liu, X.; Zhang, J.; Yang, D. Highly Efficient Gas Sensor Using a Hollow SnO_2 Microfiber for Triethylamine Detection. *ACS. Sens.* **2017**, *2*, 897−902.

(6) Wang, J.; Wan, J.; Wang, D. Hollow Multishelled Structures for Promising Applications: Understanding the Structure-Performance Correlation. *Acc. Chem. Res.* **2019**, *52*, 2169−2178.

(7) Varol, H. S.; Alvarez-Bermudez, O.; Dolcet, P.; Kuerbanjiang, B.; Gross, S.; Landfester, K.; Munoz-Espi, R. Crystallization at Nanodroplet Interfaces in Emulsion Systems: A Soft-Template Strategy for Preparing Porous and Hollow Nanoparticles. *Langmuir* **2016**, *32*, 13116−13123.

(8) Li, X.; Huang, R.; Hu, Y.; Chen, Y.; Liu, W.; Yuan, R.; Li, Z. A Templated Method to Bi_2WO_6 Hollow Microspheres and Their Conversion to Double-Shell Bi_2O_3/Bi_2WO_6 Hollow Microspheres With Improved Photocatalytic Performance. *Inorg. Chem.* **2012**, *51*, 6245−50.

(9) Cabot, A.; Ibanez, M.; Guardia, P.; Alivisatos, A. P. Reaction Regimes on The Synthesis of Hollow Particles by The Kirkendall Effect. *J. Am. Chem. Soc.* **2009**, *131*, 11326−8.

(10) Nguyen, D. T.; Kim, K.-S. Self-Development of Hollow TiO_2 Nanoparticles by Chemical Conversion Coupled with Ostwald Ripening. *Chem. Eng. J.* **2016**, *286*, 266−271.

(11) Shen, L.; Yu, L.; Yu, X. Y.; Zhang, X.; Lou, X. W. Self-Templated Formation of Uniform $NiCo_2O_4$ Hollow Spheres with Complex Interior Structures for Lithium-Ion Batteries and Supercapacitors. *Angew. Chem., Int. Ed.* **2015**, *54*, 1868−1872.

(12) Zou, F.; Hu, X.; Li, Z.; Qie, L.; Hu, C.; Zeng, R.; Jiang, Y.; Huang, Y. MOF-derived porous ZnO/ZnFe(2)O(4)/C octahedra with hollow interiors for high-rate lithium-ion batteries. *Adv. Mater.* **2014**, *26*, 6622−6628.

(13) Guo, Y.; Mei, S.; Yuan, K.; Wang, D.-J.; Liu, H.-C.; Yan, C.-H.; Zhang, Y.-W. Low-Temperature CO_2 Methanation over CeO_2-Supported Ru Single Atoms, Nanoclusters, and Nanoparticles Competitively Tuned by Strong Metal−Support Interactions and H-Spillover Effect. *ACS Catal.* **2018**, *8*, 6203−6215.

(14) An, J.; Wang, Y.; Lu, J.; Zhang, J.; Zhang, Z.; Xu, S.; Liu, X.; Zhang, T.; Gocyla, M.; Heggen, M.; Dunin-Borkowski, R. E.; Fornasiero, P.; Wang, F. Acid-Promoter-Free Ethylene Methoxycarbonylation over Ru-Clusters/Ceria: The Catalysis of Interfacial Lewis Acid-Base Pair. *J. Am. Chem. Soc.* **2018**, *140*, 4172−4181.

(15) Wu, K.; Wang, X.-Y.; Guo, L.-L.; Xu, Y.-J.; Zhou, L.; Lyu, Z.-Y.; Liu, K.-Y.; Si, R.; Zhang, Y.-W.; Sun, L.-D.; Yan, C.-H. Facile synthesis of Au embedded CuO_x-CeO_2 core/shell nanospheres as highly reactive and sinter-resistant catalysts for catalytic hydrogenation of p-nitrophenol. *Nano Res.* **2020**, *13*, 2044−2055.

(16) Zhou, H. P.; Wu, H. S.; Shen, J.; Yin, A. X.; Sun, L. D.; Yan, C. H. Thermally stable Pt/CeO(2) hetero-nanocomposites with high catalytic activity. *J. Am. Chem. Soc.* **2010**, *132*, 4998−4999.

(17) Zeng, Y.; Haw, K. G.; Wang, Y.; Zhang, S.; Wang, Z.; Zhong, Q.; Kawi, S. Recent Progress of CeO_2−TiO_2 Based Catalysts for Selective Catalytic Reduction of NO_x by NH_3. *ChemCatChem* **2020**, *13*, 491−505.

(18) Zeng, Y.; Haw, K. G.; Wang, Z.; Wang, Y.; Zhang, S.; Hongmanorom, P.; Zhong, Q.; Kawi, S. Double Redox Process to Synthesize CuO-CeO_2 Catalysts with Strong Cu-Ce Interaction for Efficient Toluene Oxidation. *J. Hazard. Mater.* **2021**, *404*, No. 124088.

(19) Yuan, K.; Guo, Y.; Huang, L.; Zhou, L.; Yin, H. J.; Liu, H.; Yan, C. H.; Zhang, Y. W. Tunable Electronic Metal-Support Interactions on Ceria-Supported Noble-Metal Nanocatalysts in Controlling the Low-Temperature CO Oxidation Activity *Inorg. Chem.* **2020**, DOI: 10.1021/acs.inorgchem.0c03219.

(20) Jia, H.; Zhu, X. M.; Jiang, R.; Wang, J. Aerosol-Sprayed Gold/Ceria Photocatalyst with Superior Plasmonic Hot Electron-Enabled Visible-Light Activity. *ACS. Appl. Mater. Interfaces* **2017**, *9*, 2560−2571.

(21) Montini, T.; Melchionna, M.; Monai, M.; Fornasiero, P. Fundamentals and Catalytic Applications of CeO_2-Based Materials. *Chem. Rev.* **2016**, *116*, 5987−6041.

(22) Mai, H. X.; Sun, L. D.; Zhang, Y. W.; Si, R.; Feng, W.; Zhang, H. P.; Liu, H. C.; Yan, C. H. Shape-selective synthesis and oxygen storage behavior of ceria nanopolyhedra, nanorods, and nanocubes. *J. Phys. Chem. B* **2005**, *109*, 24380−24385.

(23) Fu, X. P.; Guo, L. W.; Wang, W. W.; Ma, C.; Jia, C. J.; Wu, K.; Si, R.; Sun, L. D.; Yan, C. H. Direct Identification of Active Surface Species for the Water-Gas Shift Reaction on a Gold-Ceria Catalyst. *J. Am. Chem. Soc.* **2019**, *141*, 4613−4623.

(24) Li, Z.; Sibudjing, K. Facile Synthesis of Multi-Ni-Core@Ni Phyllosilicate@CeO_2 Shell Hollow Spheres with High Oxygen Vacancy Concentration for Dry Reforming of CH_4. *ChemCatChem* **2018**, *10*, 2994−3001.

(25) Kong, J.; Xiang, Z.; Li, G.; An, T. Introduce Oxygen Vacancies into CeO_2 Catalyst for Enhanced Coke Resistance During Photo-thermocatalytic Oxidation of Typical Vocs. *Appl. Catal., B* **2020**, *269*, No. 118755.

(26) May, Y. A.; Wang, W.-W.; Yan, H.; Wei, S.; Jia, C.-J. Insights into Facet-Dependent Reactivity of CuO−CeO_2 Nanocubes and Nanorods As Catalysts for CO Oxidation Reaction. *Chin. J. Catal.* **2020**, *41*, 1017−1027.

(27) Takei, D.; Yatabe, T.; Jin, X.; Yabe, T.; Mizuno, N.; Yamaguchi, K. CeO_2-Supported Pd(II)-on-Au Nanoparticle Catalyst for Aerobic Selective α,β-Desaturation of Carbonyl Compounds Applicable to Cyclohexanones. *ACS Catal.* **2020**, *10*, 5057−5063.

(28) Xiang, Y.; He, J.; Sun, N.; Fan, Y.; Yang, L.; Fang, C.; Kuai, L. Hollow Mesoporous CeO_2 Microspheres for Efficient Loading of Au Single-Atoms to Catalyze The Water-Gas Shift Reaction. *Microporous Mesoporous Mater.* **2020**, *308*, No. 110507.

(29) Fang, S.; Xin, Y.; Ge, L.; Han, C.; Qiu, P.; Wu, L. Facile Synthesis of CeO_2 Hollow Structures with Controllable Morphology by Template-Engaged Etching of Cu_2O and Their Visible Light Photocatalytic Performance. *Appl. Catal., B* **2015**, *179*, 458−467.

(30) Cao, C.-Y.; Cui, Z.-M.; Chen, C.-Q.; Song, W.-G.; Cai, W. Ceria Hollow Nanospheres Produced by a Template-Free Microwave-Assisted Hydrothermal Method for Heavy Metal Ion Removal and Catalysis. *J. Phys. Chem. C* **2010**, *114*, 9865−9870.

(31) Devaiah, D.; Reddy, L. H.; Park, S.-E.; Reddy, B. M. Ceria−zirconia mixed oxides: Synthetic methods and applications. *Catal. Rev.* **2018**, *60*, 177−277.

(32) Guo, Z.; Jian, F.; Du, F. A Simple Method to Controlled Synthesis of CeO_2 Hollow Microspheres. *Scr. Mater.* **2009**, *61*, 48−51.

(33) Zhu, Y.; Choi, S. H.; Fan, X.; Shin, J.; Ma, Z.; Zachariah, M. R.; Choi, J. W.; Wang, C. Recent Progress on Spray Pyrolysis for High Performance Electrode Materials in Lithium and Sodium Rechargeable Batteries. *Adv. Energy Mater.* **2017**, *7*, No. 1601578.

(34) Leng, J.; Wang, Z.; Wang, J.; Wu, H. H.; Yan, G.; Li, X.; Guo, H.; Liu, Y.; Zhang, Q.; Guo, Z. Advances in Nanostructures Fabricated via Spray Pyrolysis and Their Applications in Energy Storage and Conversion. *Chem. Soc. Rev.* **2019**, *48*, 3015−3072.

(35) Rahemi Ardekani, S.; Sabour Rouh Aghdam, A.; Nazari, M.; Bayat, A.; Yazdani, E.; Saievar-Iranizad, E. A Comprehensive Review on Ultrasonic Spray Pyrolysis Technique: Mechanism, Main Parameters and Applications in Condensed Matter. *J. Anal. Appl. Pyrolysis* **2019**, *141*, No. 104631.

(36) Du, H.; Huang, K.; Li, M.; Xia, Y.; Sun, Y.; Yu, M.; Geng, B. Gas Template-Assisted Spray Pyrolysis: A Facile Strategy to Produce Porous Hollow Co_3O_4 with Tunable Porosity for High-Performance Lithium-Ion Battery Anode Materials. *Nano Res.* **2018**, *11*, 1490−1499.

(37) Zhai, P.; Xu, C.; Gao, R.; Liu, X.; Li, M.; Li, W.; Fu, X.; Jia, C.; Xie, J.; Zhao, M.; Wang, X.; Li, Y. W.; Zhang, Q.; Wen, X. D.; Ma, D. Highly Tunable Selectivity for Syngas-Derived Alkenes over Zinc and Sodium-Modulated Fe_5C_2 Catalyst. *Angew. Chem., Int. Ed.* **2016**, *55*, 9902−9907.

(38) Zhang, Z.-S.; Fu, X.-P.; Wang, W.-W.; Jin, Z.; Song, Q.-S.; Jia, C.-J. Promoted porous Co_3O_4-Al_2O_3 catalysts for ammonia decomposition. *Sci. China: Chem.* **2018**, *61*, 1389−1398.

(39) Jin, Z.; Wang, F.; Wang, F.; Wang, J.; Yu, J. C.; Wang, J. Metal Nanocrystal-Embedded Hollow Mesoporous TiO_2 and ZrO_2 Microspheres Prepared with Polystyrene Nanospheres as Carriers and Templates. *Adv. Funct. Mater.* **2013**, *23*, 2137−2144.

(40) Li, L.; Tsung, C.-K.; Ming, T.; Sun, Z.; Ni, W.; Shi, Q.; Stucky, G. D.; Wang, J. Multifunctional Mesostructured Silica Microspheres from an Ultrasonic Aerosol Spray. *Adv. Funct. Mater.* **2008**, *18*, 2956−2962.

(41) Jin, Z.; Xiao, M.; Bao, Z.; Wang, P.; Wang, J. A General Approach yo Mesoporous Metal Oxide Microspheres Loaded with Noble Metal Nanoparticles. *Angew. Chem., Int. Ed.* **2012**, *51*, 6406−10.

(42) Jia, H.; Jiang, R.; Lu, W.; Ruan, Q.; Wang, J.; Yu, J. C. Aerosol-Spray Metal Phosphide Microspheres with Bifunctional Electrocatalytic Properties for Water Splitting. *J. Mater. Chem. A* **2018**, *6*, 4783−4792.

(43) Kuai, L.; Wang, J.; Ming, T.; Fang, C.; Sun, Z.; Geng, B.; Wang, J. Aerosol-Spray Diverse Mesoporous Metal Oxides from Metal Nitrates. *Sci. Rep.* **2015**, *5*, No. 9923.

(44) Yang, F.; Ding, S.; Song, H.; Yan, N. Single-atom Pd dispersed on nanoscale anatase TiO2 for the selective hydrogenation of phenylacetylene. *Sci. China Mater.* **2020**, *63*, 982−992.

(45) Zhang, B.; Sun, G.; Ding, S.; Asakura, H.; Zhang, J.; Sautet, P.; Yan, N. Atomically Dispersed Pt1-Polyoxometalate Catalysts: How Does Metal-Support Interaction Affect Stability and Hydrogenation Activity? *J. Am. Chem. Soc.* **2019**, *141*, 8185−8197.

(46) Pan, Y.; Chen, Y.; Wu, K.; Chen, Z.; Liu, S.; Cao, X.; Cheong, W. C.; Meng, T.; Luo, J.; Zheng, L.; Liu, C.; Wang, D.; Peng, Q.; Li, J.; Chen, C. Regulating The Coordination Structure of Single-Atom Fe-N_xC_y Catalytic Sites for Benzene Oxidation. *Nat. Commun.* **2019**, *10*, No. 4290.

(47) Małecka, B.; Łącz, A.; Drożdż, E.; Małecki, A. Thermal decomposition of d-metal nitrates supported on alumina. *J. Therm. Anal. Calorim.* **2015**, *119*, 1053−1061.

(48) Yang, Q.; Fu, X.-P.; Jia, C.-J.; Ma, C.; Wang, X.; Zeng, J.; Si, R.; Zhang, Y.-W.; Yan, C.-H. Structural Determination of Catalytically Active Subnanometer Iron Oxide Clusters. *ACS Catal.* **2016**, *6*, 3072−3082.

(49) Yang, C.; Zhao, H.; Hou, Y.; Ma, D. Fe_5C_2 Nanoparticles: A Facile Bromide-Induced Synthesis and as An Active Phase for Fischer-Tropsch Synthesis. *J. Am. Chem. Soc.* **2012**, *134*, 15814−15821.

(50) An, B.; Cheng, K.; Wang, C.; Wang, Y.; Lin, W. Pyrolysis of Metal−Organic Frameworks to Fe_3O_4@Fe_5C_2 Core−Shell Nanoparticles for Fischer−Tropsch Synthesis. *ACS Catal.* **2016**, *6*, 3610−3618.

(51) Tian, Z.; Wang, C.; Si, Z.; Ma, L.; Chen, L.; Liu, Q.; Zhang, Q.; Huang, H. Fischer-Tropsch Synthesis to Light Olefins over Iron-Based Catalysts Supported on $KMnO_4$ Modified Activated Carbon by A Facile Method. *Appl. Catal., A* **2017**, *541*, 50−59.

(52) Pérez-Alonso, F. J.; Herranz, T.; Rojas, S.; Ojeda, M.; López Granados, M.; Terreros, P.; Fierro, J. L. G.; Gracia, M.; Gancedo, J. R. Evolution of The Bulk Structure and Surface Species on Fe−Ce Catalysts during The Fischer−Tropsch Synthesis. *Green Chem.* **2007**, *9*, 663−670.

(53) Santos, V. P.; Wezendonk, T. A.; Jaen, J. J.; Dugulan, A. I.; Nasalevich, M. A.; Islam, H. U.; Chojecki, A.; Sartipi, S.; Sun, X.; Hakeem, A. A.; Koeken, A. C.; Ruitenbeek, M.; Davidian, T.; Meima, G. R.; Sankar, G.; Kapteijn, F.; Makkee, M.; Gascon, J. Metal Organic Framework-Mediated Synthesis of Highly Active and Stable Fischer-Tropsch Catalysts. *Nat. Commun.* **2015**, *6*, No. 6451.